Mol. Spectry. 20, 391 (1966).
[10]D. A. Stephenson and R. G. Strauch, J. Mol. Spectry. 35, 494 (1970).
[11]P. Helminger, F. C. De Lucia, and W. Gordy, Phys. Rev. Letters 25, 1397 (1970).
[12]W. Gordy, in *Molecular Spectroscopy* (Butterworths, London, 1965), Vol. VIII, pp. 403-434.
[13]F. C. De Lucia, P. Helminger, and W. Gordy, Phys. Rev. A 3, 1849 (1971).
[14]P. Helminger, R. L. Cook, and F. C. De Lucia, J. Mol. Spectry. 40, 125 (1971).
[15]R. S. Winton, Ph.D. dissertation (Duke University, 1972) (unpublished).
[16]R. S. Winton and W. Gordy, Phys. Letters 32A, 219 (1970).
[17]S. G. Kukolich, J. Chem. Phys. 50, 3751 (1969).
[18]J. K. G. Watson, J. Chem. Phys. 45, 1360 (1966); 46, 1935 (1967); 48, 4517 (1968).
[19]F. C. De Lucia, R. L. Cook, P. Helminger, and W. Gordy, J. Chem. Phys. 55, 5334 (1971).
[20]R. L. Cook, F. C. De Lucia, and P. Helminger, J. Mol. Spectry. (to be published).
[21]The relations between ($\mathfrak{a}$,$\mathfrak{B}$,$\mathfrak{C}$), (A, B, C), and (A', B', C'), have been summarized by W. Gordy and R. L. Cook, *Microwave Molecular Spectra* (Wiley-Interscience, New York, 1970), Chap. 8.
[22]D. Kivelson and E. B. Wilson, J. Chem. Phys. 21, 1229 (1953).
[23]D. E. Burch, J. Opt. Soc. Am. 58, 1383 (1968).

PHYSICAL REVIEW A VOLUME 5, NUMBER 2 FEBRUARY 1972

Combined Zeeman and High-Frequency Stark Effects, with Applications to Neutral-Helium Lines Useful in Plasma Diagnostics*

William W. Hicks, Roger A. Hess, and William S. Cooper
Lawrence Radiation Laboratory, University of California, Berkeley, California 94720
(Received 6 July 1971)

We have extended the theory of the high-frequency Stark effect in atomic spectra to treat cases of multiple interacting upper levels and of strong electric fields and resonances, where perturbation theory is inadequate. We have also included the effects of a static external magnetic field both in the perturbation theory and the more general treatment. Numerical calculations are presented for the 4922- and 4388-Å lines of He I for several field strengths and frequencies. The new theory is used to infer the frequency and strength of a microwave electric field applied to a steady-state helium discharge with no magnetic field; excellent agreement is obtained between the calculated and the observed spectra.

I. INTRODUCTION

In 1961 Baranger and Mozer proposed using the high-frequency Stark effect as a diagnostic tool to study oscillating electric fields in plasmas.[1] Such electric fields induce atomic transitions involving more than one quantum which produce "satellites" of allowed or forbidden spectral lines. The frequency (or frequency spectrum), intensity, and direction of the electric fields in the plasma can be determined from the intensities, frequencies, and polarizations of the satellites. Theoretical treatments of the high-frequency Stark effect, based on second-order time-dependent perturbation theory, have been given by Baranger and Mozer,[1] by Reinheimer,[2] and by Cooper and Ringler.[3] Cooper and Ringler also demonstrated agreement with experimental results for low electric field strengths.

There are, however, important disadvantages of the perturbation calculations mentioned above. First, it is difficult to extend them to include higher-order satellites (higher-order multiple quantum transitions) which are important at high electric field strengths and near resonances. Second, Stark shifts of the levels, which change the spectral positions of the satellites, become increasingly important as the field strength grows, and they must be calculated separately, again using perturbation theory. An approach which is valid at high field strengths or near a resonance is that of Autler and Townes,[4] which avoids the usual perturbation treatment, and which is able to calculate Stark shifts and higher multiple quantum transitions.

In the last three years, numerous authors have applied the Stark effect to the study of high-frequency electric fields in plasmas.[5-13] In two of these experiments,[8,10] the electric field strengths appear to be so high that the validity of calculations based on perturbation theory is questionable. Recognizing this, Kunze *et al.* have modified the perturbation theory by adding a phenomenological damping constant[5] and by extending the calculations of the intensities of the lowest-order satellites to fourth order.[8] Cooper and Hicks have estimated the range of validity of perturbation calculations and have pointed out possible pitfalls in using the high-frequency Stark effect in plasma diagnostics.[14]

In many laboratory plasmas in which one would like to use this spectroscopic technique, not only are strong high-frequency electric fields present, but the plasma may also be permeated by a magnetic field. This situation has not been treated by any of the theories mentioned above. Cooper and Hess[9] have pointed out one simplification introduced by the magnetic field; by simply inspecting the Zeeman pattern of the satellites it is possible to determine the relative directions of the electric and magnetic fields, and if the electric field is circularly polarized, the sense of the polarization. This technique has also been applied by Scott *et al.*[10]

There is a clear need for a comprehensive theoretical treatment of the high-frequency Stark and Stark-Zeeman effects which is valid for strong electric and magnetic fields, and for arbitrary electric field frequency. We develop such a theory in Sec. II of this paper by extending the method of Autler and Townes to include more than two upper levels and the interaction of a magnetic field with the excited atom. Unfortunately, the usefulness of the theory is somewhat restricted because the resulting set of equations must be solved by a computer. Since in many cases the perturbation theory is adequate, in Sec. III we extend it to include the effects of a magnetic field and illustrate its use in calculating the high-frequency Stark-Zeeman effect of the 4922-Å line of He I. In Sec. IV we display numerical results of the general theory, and in Sec. V we compare the theoretical calculations with experiment for the case of no magnetic field and in a situation in which the perturbation theory fails.

II. MULTILEVEL THEORY

A. Equivalence of Schrödinger's Equation to Infinite Set of Linear Equations

We start from the time-dependent Schrödinger equation for an atom in external magnetic and electric fields, and split the Hamiltonian into three parts:

$$i\dot{\psi} = H(\vec{\mathbf{r}}, t)\psi \equiv (H_0 + H_1 + H_2)\psi. \tag{1}$$

In Eq. (1) and in the rest of this paper all energies are expressed in angular frequency units. H_0 is the time-independent Hamiltonian for the unperturbed atom (no external fields) and is assumed to have a known orthonormal set of eigenfunctions $\{U_j\}$ and corresponding eigenvalues $\{\omega_j\}$:

$$H_0 U_j = \omega_j U_j, \quad j = 1, 2, \ldots . \tag{2}$$

In general, H_0 will have an infinite number of eigenfunctions, but for any single calculation only a finite number N will be physically important (their choice will be discussed in Sec. IV). H_1 represents the interaction energy between the atom and the externally applied static magnetic field $\vec{\mathbf{B}}$ and is time independent. It will often be possible to pick the $\{U_j\}$ to be eigenfunctions not only of H_0 but also of H_1. In this case

$$(H_0 + H_1)U_j = \omega_j' U_j, \quad \omega_j' \equiv \omega_j + m_j \omega_L, \tag{3}$$

where ω_L is the Larmor frequency

$$\omega_L \equiv \tfrac{1}{2}\left| eB/m_e c \right|, \quad B \equiv \left|\vec{\mathbf{B}}\right|, \tag{4}$$

and m_j is the magnetic quantum number of eigenstate j. H_2 represents the interaction energy between the atom and the externally applied electric field. The electric field is assumed to vary harmonically in time with frequency ω, thus allowing separation of the time and space dependence of H_2:

$$H_2(\vec{\mathbf{r}}, t) = H_2^+(\vec{\mathbf{r}})e^{i\omega t} + H_2^-(\vec{\mathbf{r}})e^{-i\omega t} . \tag{5}$$

We next expand the wave function

$$\psi(\vec{\mathbf{r}}, t) = \sum_{j=1}^{N} T_j(t) U_j(\vec{\mathbf{r}}), \tag{6}$$

where the T's are time-dependent coefficients to be determined. Substituting this expansion into Eq. (1) we obtain

$$i \sum_{j=1}^{N} U_j \dot{T}_j = \sum_{j=1}^{N} (\omega_j + H_1 + H_2) U_j T_j . \tag{7}$$

We multiply on the left by U_j^*, integrate over all space, and use the orthonormality of the U's to get (we interchange j and j' for convenience)

$$i\dot{T}_j = \omega_j T_j + \sum_{j'=1}^{N} (\alpha_{jj'} + \beta_{jj'}^+ e^{i\omega t} + \beta_{jj'}^- e^{-i\omega t}) T_{j'} , \tag{8}$$

where we have defined the following quantities:

$$\begin{aligned} &\alpha_{jj'} \equiv \langle j | H_1 | j' \rangle \equiv \int d^3r\, U_j^* H_1 U_{j'} , \\ &\beta_{jj'}^{\pm} \equiv \langle j | H_2^{\pm} | j' \rangle . \end{aligned} \tag{9}$$

Using Floquet's theorem of differential equations,[15] we can expand the time-dependent coefficient T_j as

$$T_j = e^{-i\lambda t} \sum_{s=-\infty}^{\infty} C_{js} e^{-is\omega t} , \tag{10}$$

where λ and the C's are time-independent unknowns; the C's are in general complex, and λ is real. Substitution of this expression for T_j into Eq. (8) yields

$$\begin{aligned} \sum_{s=-\infty}^{\infty} (\lambda + s\omega) C_{js} e^{-i(\lambda + s\omega)t} &= \sum_{s=-\infty}^{\infty} \omega_j C_{js} e^{-i(\lambda + s\omega)t} \\ &+ \sum_{j'=1}^{N} \sum_{s=-\infty}^{\infty} C_{j's} [\alpha_{jj'} e^{-is\omega t} + \beta_{jj'}^+ e^{-i(s-1)\omega t} \\ &+ \beta_{jj'}^- e^{-i(s+1)\omega t}] e^{-i\lambda t} . \end{aligned} \tag{11}$$

Since this equation must be valid for all times, we may equate coefficients of equal powers of $e^{-i\omega t}$ to give

$$(\omega_j - s\omega - \lambda) C_{js} + \sum_{j'=1}^{N} (\alpha_{jj'} C_{j's} + \beta_{jj'}^+ C_{j',s+1}$$

$$+\beta^{-}_{jj'}C_{j',s-1})=0,$$

$$j=1,2,\ldots,N,\quad s=-\infty,\ldots,+\infty. \tag{12}$$

This set of equations was solved by Autler and Townes[4] in terms of an infinitely continued fraction for the special case $N=2$, $\alpha=0$ (no magnetic field), and $\beta^{+}=\beta^{-}$ (linearly polarized electric field). As pointed out by Autler and Townes, once any single solution has been found to the set of equations (12), the new variables

$$\lambda' \equiv \lambda + m\omega,$$
$$C'_{js} \equiv C_{j,s+m},\quad j=1,\ldots,N,\quad s=-\infty,\ldots,+\infty \tag{13}$$

where m is any positive or negative integer, will also comprise a solution. We will refer to solutions related by Eqs. (13) as a "set." There are an infinite number of solutions within each set but every solution in a set contains the same physical information, i.e., corresponds to the same wave function ψ, as can be seen by noting that the expression for T_j [Eq. (10)] is invariant under the substitution given by Eqs. (13).

B. Discussion of Exact Solution

We have shown above that solving Schrödinger's equation [Eq. (1)] is equivalent to solving the infinite set of equations (12) for λ and the C's. Given a solution of Eqs. (12), substitution of λ and C_{js}, $j=1,\ldots,N$, and $s=-\infty,\ldots,\infty$, into the expression for ψ gives a solution to Eq. (1). Since the Hamiltonian H has been defined over an N dimensional space made up of the eigenstates of H_0, the complete solution of Eq. (1) must consist of N linearly independent ψ's. We have seen above that the solutions of Eq. (12) within a single set give the same wave function ψ; thus there must be N different sets of solutions to Eq. (12). We denote the different sets with the index "i":

$$\psi_i = e^{-i\lambda_i t}\sum_{j=1}^{N} C^i_{js}e^{-is\omega t}U_j,\quad i=1,\ldots,N. \tag{14}$$

Before discussing the interpretation of the wave function ψ_i, we will examine its mathematical properties and from them prove two relations between the C's which will be useful in Secs. IIC and IID. We start from Schrödinger's equation $H\psi_i = i\,\partial\psi_i/\partial t$ and its Hermitian conjugate $\psi^*_{i'}H = -i\,\partial\psi^*_{i'}/\partial t$ which together imply

$$\frac{d}{dt}\langle i'|i\rangle \equiv \frac{d}{dt}\int d^3r\,\psi^*_{i'}\psi_i = 0. \tag{15}$$

We can use Eq. (14) to evaluate ψ_i:

$$\langle i'|i\rangle = e^{-i(\lambda_i-\lambda_{i'})t}\sum_{u=-\infty}^{\infty}e^{-iu\omega t}\sum_{j=1}^{N}\sum_{s=-\infty}^{\infty}C^{i'*}_{j,s-u}C^i_{js},$$
$$u\equiv s-s'. \tag{16}$$

From the above expression we can get a useful relationship between the C's by noting that condition (15) requires that the right-hand side of Eq. (16) be independent of time. This will be true if and only if

$$\sum_{j=1}^{N}\sum_{s=-\infty}^{\infty}C^{i'*}_{j,s-u}C^i_{js} = \chi_i\,\delta_{ii'}\delta_{u0} \equiv \delta_{ii'}\delta_{u0}. \tag{17}$$

The constants $\{\chi_i\}$ are arbitrary and we have chosen them to be 1 (this choice determines the normalization of the C's).

Using (17) we can rewrite (16) as

$$\langle i'|i\rangle = \delta_{ii'}, \tag{18}$$

and thus show that at any time t the $\{\psi_i\}$ form an orthonormal set of solutions to the time-dependent Schrödinger equation. Furthermore, the $\{\psi_i\}$ form a set of stationary wave functions (the probability density $\psi^*_i\psi_i$ is independent of time when integrated over all space) and hence represent the stationary states of an atom in the presence of a static magnetic field and an oscillating electric field; by stationary we mean that an atom in state ψ_i at time $t=t_0$ will remain in that state indefinitely.

To derive a second relation similar to (17) we start by rewriting Eq. (14) as

$$\psi_i = \sum_{j=1}^{N}\tau_{ij}U_j,\quad \tau_{ij}\equiv e^{-i\lambda_i t}\sum_{s=-\infty}^{\infty}C^i_{js}e^{-is\omega t}. \tag{19}$$

Since both sets of wave functions, $\{\psi_i\}$ and $\{U_j\}$, form an orthonormal basis for the N-dimensional vector space at any time t, the matrix $\underline{\tau}$ must be unitary for all t. For a unitary matrix $\underline{\tau}$ we must have $\tau^\dagger\tau = 1$. Evaluating this condition in terms of the matrix elements τ_{ij} we have

$$\sum_{u=-\infty}^{\infty}e^{-iu\omega t}\sum_{i=1}^{N}\sum_{s=-\infty}^{\infty}C^{i*}_{j',s-u}C^i_{js} = \delta_{jj'}, \tag{20}$$

for all t. Since the right-hand side is independent of t, the left-hand side must be also. This will be true if and only if the C's satisfy the condition

$$\sum_{i=1}^{N}\sum_{s=-\infty}^{\infty}C^{i*}_{j',s-u}C^i_{js} = \delta_{jj'}\delta_{u0}. \tag{21}$$

As is shown by Eq. (19) above, the set of wave functions $\{\psi_i\}$ which solves the time-dependent Schrödinger equation represents the rearrangement of the eigenfunctions $\{U_j\}$ into a new set of functions which span the same N-dimensional space as the $\{U_j\}$. The nature of this rearrangement changes in time since $\underline{\tau}$ is a function of time, but at all times the new set of functions form an orthonormal set. We shall assume that the $\{\psi_i\}$ have been chosen such that in the limit $H_1, H_2 \to 0$, $\psi_i \to U_i$. This choice is not necessary but will lead to simplifications in Secs. IIC and IID. When no external fields are present an atom can be characterized by the set of stationary states represented by the wave functions

$\{U_j e^{-i\omega_j t}\}$. Each such state has a well-defined energy ω_j; an allowed dipole transition between two such states produces a single spectral line. In the presence of an external oscillating electric field and a static magnetic field the stationary states of the atom are represented by the $\{\psi_i\}$ or linear combinations (with time-independent coefficients) of the $\{\psi_i\}$. As can be seen from the form of the $\{\psi_i\}$ and expression (19) there is no set of states whose members are both stationary and can be characterized by a unique energy (i.e., have a simple exponential time dependence). As a result spectra produced in the presence of an oscillating electric field are more complicated than in the field-free case: A single line (allowed or forbidden) which would exist in the field-free case is replaced in the field-present case by an infinite series of spectral lines.

C. Transition Rate of Atom in Presence of Static Magnetic Field and Oscillating Electric Field

In the presence of a static magnetic field and an oscillating electric field, the state of an atom, both before and after a transition, will be described by a wave function of the form (14). However, in many cases we can assume that the final state k is negligibly affected by the electric field. As can be seen from the perturbation solution for λ and the C's [Eq. (A8) in the Appendix], this condition will occur if *all* states k' coupled to the state k by a nonzero electric dipole matrix element $\beta^{\pm}_{kk'}$ also satisfy $|\omega'_k - \omega'_{k'}| \gg |\beta^{\pm}_{kk'}|$ and ω. In addition, if we assume that a representation of the unperturbed eigenstates has been chosen such that both H_0 and H_1 are diagonal operators, then the final state k can be described by the wave function

$$\psi_k = U_k e^{-i\omega'_k t} . \tag{22}$$

We define $\mathcal{S}(\omega_\gamma)d\omega_\gamma d\Omega$ to be the number of photons emitted into solid angle $d\Omega$/sec with polarization $\hat{e}_\gamma$ and with frequencies in the range ω_γ to $\omega_\gamma + d\omega_\gamma$. In the Appendix we calculate the photon emission spectrum $\mathcal{S}^k_i(\omega_\gamma)$ for transitions from an upper state i to the lower state k of Eq. (22):

$$\mathcal{S}^k_i(\omega_\gamma) = \frac{e^2\omega_\gamma}{2\pi\hbar c^3} \sum_{s=-\infty}^{\infty} \delta(\omega'_k + \omega_\gamma - \lambda_i - s\omega) \times \sum_{j,j'=1}^{N} \omega'_{jk}\omega'_{j'k}\, \xi^k_j \xi^{k*}_{j'} C^i_{js} C^{i*}_{j's}, \tag{23}$$

$\omega'_{jk} \equiv \omega'_j - \omega'_k$. The matrix element ξ^k_j contains the dependence of the transition rate on the direction and polarization of the emitted photon and is defined in Sec. III, Eq. (36). The total photon emission spectrum $\mathcal{S}$ from an ensemble of N_a atoms populating the N states $\{\psi_i\}$ will be expression (23) summed over final states, averaged over initial states, and summed over photon polarization:

$$\mathcal{S}(\omega_\gamma) = \sum_{e_\gamma} \sum_{i=1}^{N} K_i \sum_{k=1}^{N'} \mathcal{S}^k_i, \quad K_i \equiv \frac{N_i}{N_a} . \tag{24}$$

Here N_i is the number of atoms in the state i, N' is the number of final states, and K_i represents the probability that the state i is occupied by atoms in the ensemble and has the normalization

$$\sum_{i=1}^{N} K_i = 1. \tag{25}$$

The value given to K_i in any particular problem will be governed by physical considerations. In the calculations presented in Secs. III and IV we have assumed that

$$K_i = 1/N, \quad i = 1, \ldots, N \tag{26}$$

i.e., that each of the states ψ_i is equally populated by atoms in the ensemble. In the limit of no external fields where $\psi_i \to U_i$, Eq. (26) is just the assumption that the N eigenstates $\{U_i\}$ are in thermal equilibrium at a high temperature. Such a situation occurs in most laboratory plasmas when random collisions (and not radiative transitions) are the dominant mechanism inducing transitions among states with different values of i and when the average kinetic energy of the colliding particles is large compared with the interlevel energy spacing of the N states. Then the energy levels are "degenerate" with respect to collisional excitation and deexcitation, and the effect of collisions will be to maintain equal populations. In the presence of external fields, energy levels of the N states are shifted relative to each other by energies of the order of ω and $\lambda_i - \omega_i$ (the latter quantity will be shown in Sec. III to be of the order of ω_L and $\sum_j |\beta^{\pm}_{ij}|^2/\omega'_{ij}$), but we still expect collisional processes to maintain equal populations if the mean kinetic energy of the colliding particles is much greater than these energy shifts. We can make the analogy of assumption (26) and high-temperature thermal equilibrium more explicit by considering a consequence of Eq. (26). From Eq. (19), the probability that an atom in the state i is *also* in the eigenstate U_j is

$$|\tau_{ij}|^2 = \sum_{u=-\infty}^{\infty} e^{-iu\omega t} \sum_{s=-\infty}^{\infty} C^{i*}_{j,s-u} C^i_{js} \tag{27}$$

and is time dependent. Then W_j, the probability that the eigenstate j is populated by the atoms in the ensemble, is given by Eq. (27) averaged over the states i:

$$W_j = \sum_{u=-\infty}^{\infty} e^{-iu\omega t} \sum_{i=1}^{N} K_i \sum_{s=-\infty}^{\infty} C^{i*}_{j,s-u} C^i_{js} = \frac{1}{N} ; \tag{28}$$

the latter equality follows from Eqs. (26) and (21). Thus Eq. (26) implies that the probability that the spatial eigenstate j is populated by atoms in the entire ensemble is time independent and the same for all j even though the probability that a single parti-

cle in the stationary state i is in the spatial eigenstate j is time dependent.

D. Physical Model

We now construct a physical model of the time-averaged behavior of an ensemble of atoms in the presence of a time-varying electric field. Such a model is useful in describing the solution to the Schrödinger equation (14) in terms of simple physical processes between the atom and the oscillating electric field and leads to correct theoretical predictions of atomic spectra when the variation of the differential transition rate [Eq. (A5) in the Appendix] over times of the order of ω^{-1} can be ignored. We first note that from Eq. (16) (setting $i' = i$),

$$\langle i|i\rangle = \sum_{j=1}^{N} \sum_{s=-\infty}^{\infty} |C_{js}^{i}|^2 = 1, \tag{29}$$

where we have used Eq. (17) to simplify the result. We can also calculate the energy of a particle in state ψ_i:

$$\langle i|H|i\rangle \equiv \int d^3r\, \psi_i^* i \frac{\partial}{\partial t} \psi_i$$

$$= \sum_{j=1}^{N} \sum_{s=-\infty}^{\infty} \left(\lambda_i |C_{js}^{i}|^2 + s\omega \sum_{u=-\infty}^{\infty} e^{-iu\omega t} C_{j,s-u}^{i*} C_{js}^{i} \right). \tag{30}$$

The particle energy oscillates in time due to the interaction of the atom and the external electric field. If we average Eq. (30) over the period of the electric field, $T = 2\pi/\omega$, we get

$$\frac{1}{T}\int_0^T dt \langle i|H|i\rangle = \sum_{j=1}^{N} \sum_{s=-\infty}^{\infty} |C_{js}^{i}|^2 (\lambda_i + s\omega). \tag{31}$$

We could equally well obtain the above equation by using the following model. We consider an ensemble of atoms populating the state i. We assume that each atom in the ensemble has "eigenstates" characterized by the "quantum numbers" (i, j, s); such a state has a spatial dependence U_j and an energy $\lambda_i + s\omega$. The probability that the state (i, j, s) is populated by atoms in the ensemble is assumed to be $|C_{js}^{i}|^2$. In this model Eq. (29) represents the normalization for the probability and Eq. (31) represents the ensemble-averaged energy. If we extend our ensemble to include atoms in the states $\{\psi_i, i = 1, \ldots, N\}$, then the probability of the state (i, j, s) in the enlarged ensemble will be $|C_{js}^{i}|^2$ multiplied by the probability that the state i is populated, i.e., K_i, and the average energy of an atom in the enlarged ensemble will be

$$E_{av} = \sum_{i=1}^{N} \sum_{j=1}^{N} \sum_{s=-\infty}^{\infty} K_i |C_{js}^{i}|^2 (\lambda_i + s\omega). \tag{32}$$

Atoms in the ensemble undergo transitions between the states $\{(i, j, s),\ i = 1, \ldots, N,\ j = 1, \ldots, N,$ and $s = -\infty, \ldots, +\infty\}$ owing to interactions with quanta of the external electric field. An interaction consists of the emission (absorption) of a quantum; the new state (i', j', s') after the interaction will have $i' = i$ (each state i is stationary) and $s' = s - 1$ ($s' = s + 1$), i.e., its energy after the interaction will have been decreased (increased) by the quantum energy. Since the field quanta carry angular momentum of 1 (in units of $\hbar$), the state after an interaction will differ in the index j from the state before the interaction ($\Delta l \equiv l' - l = \pm 1$, $l \equiv$ orbital angular momentum of the spatial eigenstate U_j).

In this model the energy of the state (i, j, s), $\lambda_i + s\omega$, has the following interpretation: The energy difference between ω_i (the energy of state i in the limit $H_1, H_2 \to 0$) and $\lambda_i + s\omega$ is the result of the Stark shift of the energy levels, the Zeeman splitting, and the exchange of quanta with the electric field. We assume that a representation of the $\{U_j\}$ can be found such that both H_0 and H_1 are diagonal; then the Zeeman shift of state i is $m_i\omega_L$. We must now decide which member of each set of solutions to choose for each ψ_i. From Eqs. (13) it is clear that each member of the set will have a different value of λ_i. If we choose that solution in each set for which $\Delta E \equiv \lambda_i - m_i\omega_L - \omega_i$ goes to zero when the electric field goes to zero, then we can interpret ΔE as the Stark shift, and s as the net number of electric field quanta absorbed or emitted by the atom in the state (i, j, s). Under this assumption as the electric field goes to zero, we have

$$C_{js}^{i} \to \delta_{ij}\delta_{s0}, \quad \lambda_i \to \omega_i + m_i\omega_L\,. \tag{33}$$

We can now see the significance of this particular choice. Another member of the set would have the property that a different coefficient $C_{j\sigma}^{i}$ ($\sigma \neq 0$) would remain finite in the weak-field limit. Such a situation would not change the physics, since $\lambda_i + \sigma\omega$ is invariant for all members of a set, but would not yield such a simple interpretation; $s - \sigma$ would be the net number of quanta absorbed or emitted in state (i, j, s).

Finally, we note that an atom in the state (i, j, s) can undergo a spontaneous radiative transition to a state with lower energy with which it has a nonzero dipole moment. In such a transition, the energy of the resultant photon will be $\lambda_i + s\omega$ minus the energy of the final state; hence, the optical spectra of atoms in an oscillating electric field will consist of "satellites," a given satellite being determined by fixed values of i, j, and s. The intensity of such a satellite would be given by $K_i |C_{js}^{i}|^2$ times the transition rate from U_j to the lower state. However, as can be seen from the correct expression for the total photon emission spectrum (24), this simplified model only works in the special case that we can ignore cross terms (those with $j' \neq j$) in Eq. (23). Circumstances under which cross terms

can be ignored often occur and are discussed in the Appendix.

III. EXTENSION OF PERTURBATION THEORY TO INCLUDE STARK SHIFTS AND MAGNETIC FIELD EFFECTS

A. Transition Rate for Two-Quantum Transitions in Nonhydrogenic Atoms

If we consider the weak-electric-field limit of the wave function of Eq. (14), then we can derive an expression for the transition rate which is valid for weak electric fields and which is the generalization of Eq. (1) of Cooper and Ringler[3] to include a static magnetic field and Stark shifts. We assume that the magnetic field $\vec{B}$ lies in the $\hat{z}$ direction. We consider three atomic states: i, j, and k; an electric dipole transition from i directly to k is assumed to be forbidden. In the presence of an oscillating electric field $\vec{E}$, an atom in the state i may be pictured as decaying to the state k by a two-quantum transition in which it exchanges a quantum of energy $\hbar\omega$ with the electric field, exists transiently in the intermediate state j, and undergoes a dipole transition to the state k with the emission of a photon of energy $\hbar\omega_\gamma$. The photon emission spectrum $\mathcal{S}_i^k(\omega_\gamma)$ for the photon emitted in a two-quantum transition as described above is

$$\mathcal{S}_i^k(\omega_\gamma) = \frac{e^2\omega_\gamma}{2\pi\hbar c^3}\,\delta(\omega_\gamma - \omega'_{ik} - \omega_i^S \mp \omega) \times \sum_j \frac{\omega'^2_{jk}}{(\omega'_{ij} \pm \omega)^2}\,|\beta_{ji}^{\mp}|^2\,|\xi_j^k|^2 . \quad (34)$$

This equation is the weak-electric-field limit of Eq. (23); its derivation and a discussion of the assumptions made in deriving it are given in the Appendix. In the above expression the upper sign corresponds to absorption of a quantum from the electric field, the lower sign to emission of a quantum to the electric field; ω_i^S is the second-order correction to the energy of atomic state i due to the Stark shift (the Stark shift of state k is assumed negligible),

$$\omega_i^S = \sum_{j'} \left[\frac{|\beta_{j'i}^-|^2}{(\omega'_{ij'} + \omega)} + \frac{|\beta_{j'i}^+|^2}{(\omega'_{ij'} - \omega)}\right] , \quad (35)$$

and the summation is over all intermediate states j.

The matrix elements $\beta_{ij}^{\pm}$ are proportional to the electric field strength; they are defined in Sec. II, Eq. (9) and expressions for them are given by Eqs. (57) and (58) for linearly and circularly polarized electric fields. The matrix element ξ_j^k is defined by

$$\xi_j^k \equiv \int d^3r\, U_k^*\, \hat{e}_\gamma^* \cdot \vec{r}\, U_j , \quad (36)$$

where $\vec{r}$ is the position vector of the electron, $\hat{e}_\gamma$ is a unit vector in the direction of polarization of the emitted photon, and U_j is the spatial part of the eigenfunction of the state j.

B. Special Cases

We will restrict our discussion to transitions between states with quantum numbers:

$$\begin{aligned} i &\to (n, l, m), && m = -l, \ldots, l \\ j &\to (n, l-1, m''), && m'' = -l+1, \ldots, l-1 \\ k &\to (n', l-2, m'), && m' = -l+2, \ldots, l-2. \end{aligned} \quad (37)$$

This includes most transitions of interest in plasma diagonostics. Now consider two special cases: First, a linearly polarized electric field whose azimuthal angle with respect to $\vec{B}$ is random in time and, second, an electric field which is circularly polarized and perpendicular to $\vec{B}$. In either case, due to the time-averaged azimuthal symmetry of the electric field, we can average over the azimuthal angle in evaluating $|\xi_j^k|^2$. If the photon is emitted at an angle θ with respect to $\vec{B}$, then for photon polarization parallel to B ("π" polarization) we have

$$|\xi_j^k|^2 = \tfrac{1}{2}\left(|x_j^k|^2 + |y_j^k|^2\right)\cos^2\theta + |z_j^k|^2\sin^2\theta , \quad (38)$$

and for polarization perpendicular to B ("σ" polarization) we have

$$|\xi_j^k|^2 = \tfrac{1}{2}\left(|x_j^k|^2 + |y_j^k|^2\right); \quad (39)$$

x_j^k, y_j^k, and z_j^k are the matrix elements of the corresponding coordinates.

1. *Linearly Polarized Electric Field*

We first consider a linearly polarized electric field

$$\vec{E}(t) = \vec{E}_0 \cos\omega(t - t_0), \quad |\vec{E}_0| = \sqrt{2}\, E_{\rm rms}. \quad (40)$$

If ζ is the angle between the electric field and the magnetic field, then after averaging over the corresponding azimuthal angle, we have

$$|\beta_{ij}^-|^2 = |\beta_{ij}^+|^2 = \frac{e^2E_{\rm rms}^2}{2\hbar^2}\left[\tfrac{1}{2}\left(|x_i^j|^2 + |y_i^j|^2\right)\sin^2\zeta + |z_i^j|^2\cos^2\zeta\right]. \quad (41)$$

To obtain $\mathcal{S}_{nl}^{n'l-2}(\omega_\gamma)$, the total photon emission spectrum for two-quantum transitions from the states $\{(n, l, m),\ m = -l, \ldots, l\}$ to the states $\{(n', l-2, m'),\ m' = -l+2, \ldots, l-2\}$, we must average Eq. (34) over the initial states i which, for simplicity, are assumed to be equally populated, sum over the final states k, and sum over both polarizations. After evaluating all matrix elements and performing the summations, we can write $\mathcal{S}_{nl}^{n'l-2}(\omega_\gamma)$ as

$$S_{nl}^{n'l-2}(\omega_\gamma)=\frac{1}{480\pi}\frac{e^4}{\hbar^3c^3}\frac{1}{g_i}E_{\rm rms}^2\frac{l(l-1)}{(2l-1)}\left|R_{nl}^{nl-1}\right|^2\left|R_{nl-1}^{n'l-2}\right|^2\left\{\left[\frac{\cos^2\zeta}{(\omega_{ij}\pm\omega)^2}\,(16\epsilon_{0,0}\sin^2\theta+6\epsilon_{0,-1}\cos^2\theta+6\epsilon_{0,1}\cos^2\theta)\right.\right.$$
$$+\frac{\sin^2\zeta}{(\omega_{ij}\pm\omega-\omega_L)^2}\,(6\epsilon_{-1,-1}\cos^2\theta+\epsilon_{-1,1}\cos^2\theta+6\epsilon_{-1,0}\sin^2\theta)+\frac{\sin^2\zeta}{(\omega_{ij}\pm\omega+\omega_L)^2}\,(6\epsilon_{1,1}\cos^2\theta+\epsilon_{1,-1}\cos^2\theta+6\epsilon_{1,0}\sin^2\theta)\Big]_{\pi F}$$
$$\left.+\left[\frac{\cos^2\zeta}{(\omega_{ij}\pm\omega)^2}(6\epsilon_{0,-1}+6\epsilon_{0,1})+\frac{\sin^2\zeta}{(\omega_{ij}\pm\omega-\omega_L)^2}\,(6\epsilon_{-1,-1}+\epsilon_{-1,1})+\frac{\sin^2\zeta}{(\omega_{ij}\pm\omega+\omega_L)^2}\,(6\epsilon_{1,1}+\epsilon_{1,-1})\right]_{\sigma F}\right\}. \quad (42)$$

We have evaluated the necessary matrix elements by using expressions from Bethe and Salpeter.[16] $R_{nl}^{n'l'}$ is an integral over the radial eigenfunctions,

$$R_{nl}^{n'l'}\equiv\int r^3dr\,R_{n'l'}(r)R_{nl}(r)\ , \quad (43)$$

and g_i is the statistical weight of the state i. The coefficients $\epsilon_{m_{ij},m_{jk}}$ are defined as

$$\epsilon_{m_{ij},m_{jk}}\equiv\omega'_{ik}\omega'^2_{jk}\delta(\omega_\gamma-\omega'_{ik}-\omega_i^S\mp\omega)\ , \quad (44)$$

where $m_{jk}\equiv m_j-m_k$, etc. As can be seen from Eq. (44) a term in Eq. (42) proportional to $\epsilon_{m_{ij},m_{jk}}$ produces a component of the Stark-Zeeman pattern with frequency

$$\omega_\gamma=\omega_{ik}+\omega_i^S\pm\omega+(m_{ij}+m_{jk})\omega_L\ . \quad (45)$$

Spectral lines described by terms within $[\cdots]_{\pi F}$ in Eq. (42) are polarized parallel to $\vec{B}$; those from terms within $[\cdots]_{\sigma F}$ are polarized perpendicular to $\vec{B}$. The "F" in the subscripts indicates that a dipole transition from $i\to k$ is forbidden. Equation (42) is the generalization of Eq. (7) of Ref. 3; it implies the usual two "satellites" of the forbidden line, each Stark shifted and split into a Zeeman pattern. If $\omega_i>\omega_j$, $+\omega$ gives the "far satellite" and $-\omega$ gives the "near satellite," each named according to its proximity to the allowed line ($j\to k$).

Two conclusions about the Stark-Zeeman pattern can be drawn from Eq. (42). First, for a given direction of observation θ, as the angle between the electric and the magnetic fields is varied from 0 to $\frac{1}{2}\pi$, some components will appear and others will disappear. It is therefore possible, as has already been pointed out,[9] to *tell the angle between the electric field and the magnetic field by simple inspection of the Zeeman pattern of the satellites.* Second, the total intensity of a satellite (the sum of the intensities of all Zeeman components) will depend on ω_L and therefore on B. For components with $m_{ij}=0$, the magnetic field dependence is very weak since $\omega'_{ik}\approx\omega_{ik}$ and $\omega'_{jk}\approx\omega_{jk}$ (the angular frequency separation between the states i, j and the state k is approximately 4×10^{15} rad/sec—in the optical frequency range—which is the value of the Larmor frequency for $B\approx10^8$ G). For components with $m_{ij}\neq0$, the magnetic field dependence will be significant if ω_L is of the same order of magnitude as the other terms in the resonant denominators in Eq. (42).

2. *Circularly Polarized Electric Field*

We now consider an electric field which is circularly polarized and perpendicular to $\vec{B}\equiv B\hat{z}$:

$$\vec{E}(t)=E_{\rm rms}(\hat{x}\cos\omega t\pm\hat{y}\sin\omega t)\ . \quad (46)$$

The upper sign corresponds to right-hand circular polarization (electric field rotation in the same sense as a free electron in the magnetic field) and will be denoted by RHC; the lower sign corresponds to left-hand circular polarization (electric field rotation in the same sense as a free positive ion) and will be denoted by LHC. A calculation similar to that given above for the linearly polarized electric field will give the transition rate. However, it is simpler to note that the matrix elements given by Eq. (58) produce the following selection rules for transitions from state i to state j via absorption or emission of a quantum of the electric field: If the electric field is RHC and a field quantum is emitted, or if $\vec{E}$ is LHC and a field quantum is absorbed, $m_{ij}=+1$; if $\vec{E}$ is RHC and a field quantum is absorbed, or if $\vec{E}$ is LHC and a field quantum is emitted, $m_{ij}=-1$. In either case, m_{jk} is unaffected and may be 0 or ±1. With these selection rules the photon emission spectrum for circularly polarized electric fields can be easily found from Eq. (42) by the following prescription: (a) Set $\zeta=\frac{1}{2}\pi$. (b) Multiply the right-hand side by 2. (c) Retain only those terms which fit the selection rules given above. For instance, if the electric field is RHC, then select only those terms with $+\omega$ in the resonant denominator and $m_{ij}=-1$ in the coefficient ϵ for the far satellite (absorption of a quantum from the field), and only those terms with $-\omega$ and $m_{ij}=+1$ for the near satellite (emission of a quantum to the field). As in Sec III B 1 above, "far" and "near" refer to the special choice $\omega_i>\omega_j$. (d) The resulting expression will be $S_{nl}^{n'l-2}$ and can be written in a form similar to (42).

C. Ratio of Intensity of Satellite to Intensity of Allowed Line

It is convenient to calculate and useful to know not only the absolute intensity of a satellite but also the ratio of the intensity of a nearby allowed transi-

tion. We can write the photon emission spectrum of the allowed dipole transition $(j \rightarrow k)$ in a fashion similar to (42):

$$s^{n'l-2}_{nl-1}(\omega_\gamma) = \frac{e^2}{2\pi\hbar c^3}\frac{1}{g_j}(l-1)\left|R^{n'l-2}_{nl-1}\right|^2 \times\{[\eta_1\cos^2\theta+\eta_{-1}\cos^2\theta+2\eta_0\sin^2\theta]_{\pi A} +[\eta_1+\eta_{-1}]_{\sigma A}\}, \quad (47)$$

where $\eta_{m_{jk}} = \omega'^3_{jk}\delta(\omega_\gamma - \omega'_{jk} - \omega^S_{jk})$. A term in Eq. (47) proportional to $\eta_{m_{jk}}$ produces a Zeeman component of the allowed transition with frequency $\omega_\gamma = \omega_{jk} + \omega^S_{jk} + m_{jk}\omega_L$. The same convention for the polarization of the emitted photon applies; the subscript A signifies "allowed."

We define $S_\pm(\theta, \zeta)$ to be the ratio of the number of photons emitted per second in "forbidden" transitions $(i \rightarrow k)$ into the solid angle $d\Omega$ to the number emitted per second in "allowed" transitions $(j \rightarrow k)$ into the solid angle $d\Omega$:

$$S_\pm(\theta, \zeta) = \frac{N_i d\Omega \int d\omega_\gamma s^k_i(\omega_\gamma)}{N_j d\Omega \int d\omega_\gamma s^k_j(\omega_\gamma)}; \quad (48)$$

N_i represents the population of state i, etc., and the upper (lower) sign corresponds to the upper (lower) sign in expression (42). If we assume that the states i, j are in thermal equilibrium in the high-temperature limit $(kT \gg |\omega'_{ij}|)$ then $N_i/N_j = g_i/g_j$, and $S_\pm(\theta, \zeta)$ reduces to

$$S_\pm(\theta, \zeta) = \frac{e^2E^2_{\rm rms}}{240\hbar^2}\frac{l}{(2l-1)}\left|R^{n'l-1}_{nl}\right|^2 \times \frac{\int d\omega_\gamma\{[\cdots]_{\pi F}+[\cdots]_{\sigma F}\}}{\int d\omega_\gamma\{[\cdots]_{\pi A}+[\cdots]_{\sigma A}\}}. \quad (49)$$

The square brackets are the same as in Eqs. (42) [or the equation equivalent to (42) in the case of a circularly polarized electric field] and (47). By using only selected terms within these brackets, one can use Eq. (49) to compare the intensity of any forbidden component with any allowed component.

As an example of the use of Eq. (49) we show in Fig. 1 the results of calculating the ratio of the intensities of components of the Zeeman pattern of the satellites of the forbidden line $(4\,^1F \rightarrow 2\,^1P)$ to the intensity of the central "π" component $(m_{jk} = 0)$ of the 4922-Å allowed line of He I $(4\,^1D \rightarrow 2\,^1P)$ for various configurations of electric and magnetic fields with $\theta = \frac{1}{2}\pi$, $\omega_{ij} = 5.63$ cm^{-1} ($4\,^1D - 4\,^1F$ separation in He I), $\omega = 2.35$ cm^{-1} (electric field frequency = 70.5 GHz), $\omega_L = 0.33$ cm^{-1} ($|\vec{B}| = 7$ kG), and $E_{\rm rms} = 1$ kV/cm.

We now discuss each part of Fig. 1 in turn.

(a) We have $\vec{E} \parallel \vec{B}$; $\zeta = 0$. The remaining nonzero terms in Eq. (42) are only very weakly dependent on $|\vec{B}|$ through ω'_{ik} and ω'_{jk}. The pattern resembles a normal Zeeman triplet, with the σ components of each satellite $\frac{3}{8}$ of the intensity of the π component.

(b) $\vec{E} \perp \vec{B}$ and is random in azimuth; $\zeta = \frac{1}{2}\pi$. The intensities of all forbidden components depend on $|\vec{B}|$ through resonant denominators; the net effect is to increase the total intensity of a satellite (the sum of the intensities of all Zeeman components) by a factor of

$$F = \frac{1}{2}\left[\left(\frac{\omega_{ij}\pm\omega}{\omega_{ij}\pm\omega+\omega_L}\right)^2+\left(\frac{\omega_{ij}\pm\omega}{\omega_{ij}\pm\omega-\omega_L}\right)^2\right] \quad (50)$$

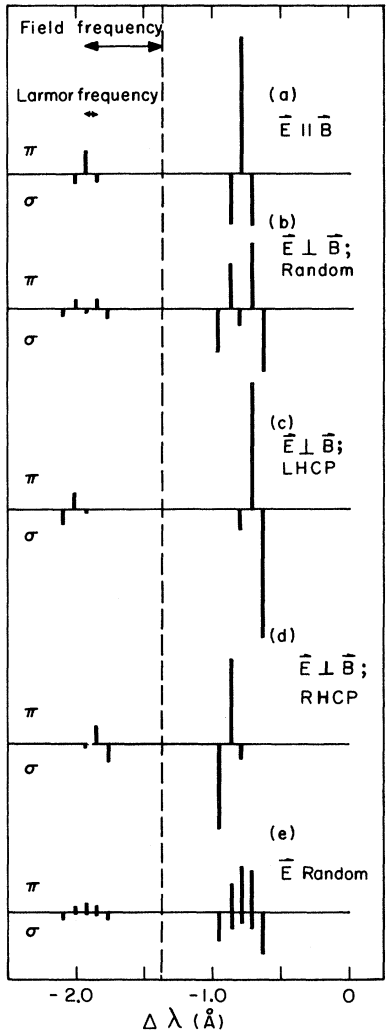

FIG. 1. Normal Zeeman patterns of the satellites of the forbidden transition $4\,^1F \rightarrow 2\,^1P$ of He I, calculated from perturbation theory and showing both σ and π polarization for various configurations of the electric field, all for direction of observation perpendicular to $\vec{B}$, field frequency of 2.35 cm^{-1}, and magnetic field strength of 7 kG. $\Delta\lambda = 0$ corresponds to the allowed line $4\,^1D \rightarrow 2\,^1P$; the vertical dashed line denotes the position of the forbidden $4\,^1F \rightarrow 2\,^1P$ transition. Shown are (a) $\vec{E}$ parallel to $\vec{B}$, (b) $\vec{E}$ perpendicular to $\vec{B}$ and random in azimuth, (c) $\vec{E}$ perpendicular to $\vec{B}$ and left-hand circularly polarized, (d) $\vec{E}$ perpendicular to $\vec{B}$ and right-hand circularly polarized, and (e) $\vec{E}$ random in direction.

over its intensity in the absence of a magnetic field. In the limit $\vec{B} \to 0$, the stronger σ components of a satellite become equal in intensity to the π components, and the weakest (central) σ component approaches $\frac{1}{3}$ the intensity of either of the other two σ components.

(c) and (d) $\vec{E} \perp \vec{B}$ and is circularly polarized. The intensities of all forbidden components again depend on B through resonant denominators. In the limit $B \to 0$, the intensities of the π component and the stronger σ component become equal; the weaker σ component approaches $\frac{1}{6}$ of the intensity of the stronger σ component.

(e) Finally, if $\vec{E}$ is entirely random in direction we must replace $\cos^2\zeta$ and $\sin^2\zeta$ in Eqs. (42) and (47) by their average values

$$\langle \sin^2\zeta \rangle_{\rm av} = (1/4\pi) \int \sin^2\zeta \, d\Omega = \tfrac{2}{3} ,$$

$$\langle \cos^2\zeta \rangle_{\rm av} = (1/4\pi) \int \cos^2\zeta \, d\Omega = \tfrac{1}{3} .$$

With these substitutions, Eq. (49) reduces in the limit $B \to 0$ to the expression for random fields ($\bar{S}_\pm$) given by Baranger and Mozer [Ref. 1, Eq. (1)]:

$$\bar{S}_\pm = \frac{e^2 a_0^2}{6\hbar^3} \, \frac{l}{(2l-1)} \, \frac{E_{\rm rms}^2 \, |R_{nl}^{nl-1}|^2}{(\omega_{ij} \pm \omega)^2} . \tag{51}$$

If $\omega \to 0$, the Zeeman patterns of the two satellites merge; the resulting pattern consisting of three π components and five σ components is the Zeeman pattern of the "forbidden line" produced by the quasistatic fields of the ions in a plasma.

Several authors have treated the dc Stark-Zeeman effect, among them Brochard and Jacquinot,[17] who derived the same selection rules as given above and calculated the Zeeman pattern of the forbidden line, and Deutsch *et al.*,[18] who have performed extensive machine calculations on the dc Stark-Zeeman effect in HeI.

IV. NUMERICAL CALCULATIONS

In this section we present results of numerical calculations using the theory given in Sec. II.

We do not have an analytical solution to the infinite set of equations (12). Instead, we use a numerical method of solution suggested by the physical interpretation.

For weak electric fields, the multiple absorption of s photons becomes less likely as $|s|$ increases (negative values of s correspond to emission) since the larger values of $|s|$ correspond to higher-order terms in the perturbation series. The probability of the absorption of one photon is given by second-order perturbation theory, two photons by third-order theory, etc. As the strength of the electric field increases, the probability of multiple absorption also increases, and higher-order satellites will become observable. However, it is reasonable to assume that even for strong fields the probability of absorbing s photons becomes negligible for $|s|$ sufficiently large. Since this probability is proportional to $|C_{js}|^2$ we assume that

$$C_{js} = 0 \quad \text{for} \quad |s| > S, \quad j = 1, 2, \ldots, N . \tag{52}$$

Then the infinite set of equations (12) is reduced to a finite set:

$$\sum_{j'=1}^{N} (\alpha_{jj'} C_{j's} + \beta_{jj'}^{+} C_{j',s+1} + \beta_{jj'}^{-} C_{j',s-1}) + (\omega_j - s\omega - \lambda) C_{js} = 0 ,$$
$$j = 1, 2, \ldots, N ,$$
$$s = -S, \ldots, +S . \tag{53}$$

Equations (53) can be viewed as an eigenvalue equation:

$$\underline{X} \, \vec{D} = \lambda \vec{D} , \tag{54}$$

where $\vec{D}$ is an $N(2S+1)$-dimensional column vector whose elements are in a one-to-one correspondence with the coefficients C_{js}, $j = 1, 2, \ldots, N$ and $s = -S, \ldots, +S$; $\underline{X}$ is an $N(2S+1) \times N(2S+1)$ matrix whose elements are chosen so that the set of equations represented by (54) is the same set given in (53). One can easily show that $\underline{X}$ is Hermitian when H is Hermitian. Let $\underline{Z}$ represent the unitary matrix which diagonalizes $\underline{X}$; we have

$$\underline{Z}^{\dagger} \underline{X} \, \underline{Z} = \underline{X}' , \tag{55}$$

where $\underline{X}'$ is the diagonal matrix whose nonzero elements are the eigenvalues of $\underline{X}$ and also the solutions for λ. The columns of $\underline{Z}$ are the eigenvectors of $\underline{X}$; they are solutions for $\vec{D}$ and hence for the C's. We can construct a solution for Eq. (1) from each of the $N(2S+1)$ eigenvalues and eigenvectors of $\underline{X}$. As discussed above, only N of these solutions are to be used in the complete wave function and, as before, the solutions may be divided into N sets, each set now containing $2S+1$ members. For the infinite set of equations (12), all of the solutions within a set can be found from any one member of the set by using the transformation (13); this will only be approximately true in the case of the finite set of equations (53) because of the approximation made in truncating the matrices. We must be careful in selecting which eigenvalues and eigenvectors to use. As one method we could choose the solution in each set most accurately fulfilling condition (52) above, or we could choose the solution described in the previous section where s has the physical meaning of the net number of photons absorbed or emitted and $\lambda_i - \omega_L m_i - \omega_i$ is the Stark shift. For low electric fields these two choices will be the same.

In order to identify which eigenstates of H_0 need

to be included in the expansion of the wave function ψ, it is helpful to consider the perturbation solution, Eq. (34). Because of the resonant denominators, for a given initial state i, the most important intermediate states j to consider are those for which $|\omega'_{ij}| - \omega$ is smallest and β_{ij} is nonzero. However, for strong electric fields, all nearly intermediate states should be included even if β_{ij} is zero, since multiple quantum transitions may be important and two states i and j can be coupled through other intermediate states. For instance, for the 4388-Å He I ($5\,^1D \rightarrow 2\,^1P$) line the $5G$ level must also be included, since it introduces satellites and strongly affects the position and intensities of the satellites originating from the $5D$ and $5F$ levels. If there are intermediate states for which $|\omega'_{ij}| \lesssim \omega$ and β_{ij} is nonzero, then states for which $|\omega'_{ij}| \gg \omega$ can be neglected unless very strong fields are present or great accuracy is desired. The best method to determine whether a particular state need be included is to perform the calculations with and without the state and compare results. Similarly the appropriate value for S [the limit of the summation in expansion (12)] can be found by increasing its value and noting the effect on the results.

In order to calculate the matrices α and $\beta^{\pm}$, and the unperturbed energy levels ω_j, we need to know the unperturbed wave functions $\{U_j\}$. Since, except for hydrogen, these wave functions are not known exactly, an approximation must be made. In many cases hydrogenic wave functions may be used to calculate the dipole matrix elements α and $\beta^{\pm}$, and measured values may be used for the unperturbed energy levels.

For hydrogenic wave functions the H_1 term is diagonal if the external magnetic field is chosen along the z axis. If the total electron spin of the atom is zero, then $H_1 = \omega_L L_z$, where L_z is the z component of the orbital angular momentum of the excited electron. H_2, the interaction energy of the high-frequency electric field, is

$$H_2 = -(\vec{\mu}\cdot\vec{E}/\hbar) = +|e|(\vec{r}\cdot\vec{E}/\hbar)\ , \tag{56}$$

where $\vec{\mu}$ is the electric dipole moment. For linear polarization of the electric field, $\vec{E}(t) = \vec{E}_0 \cos\omega t$ and

$$\beta^{+}_{jj'} = \beta^{-}_{jj'} = (|e|/2\hbar)\langle j|\vec{r}\cdot\vec{E}_0|j'\rangle\ . \tag{57}$$

For circular polarization perpendicular to the magnetic field, $\vec{E}(t) = E_{\rm rms}(\hat{x}\cos\omega t \pm \hat{y}\sin\omega t)$ and

$$\begin{aligned}\beta^{+}_{jj'} &= (|e|E_{\rm rms}/2\hbar)\langle j|x \mp iy|j'\rangle\ ,\\ \beta^{-}_{jj'} &= (|e|E_{\rm rms}/2\hbar)\langle j|x \pm iy|j'\rangle\ .\end{aligned} \tag{58}$$

The upper sign corresponds to right-hand circular polarization and the lower sign corresponds to left-hand circular polarization relative to the magnetic field.

We have confined our calculations to helium, but the theory can be used for any element, as long as the unperturbed energy levels are known to sufficient accuracy and the necessary matrix elements can be computed.

We have used our theory to investigate extensively two optical transitions of parahelium, the 4922-Å ($4\,^1D \rightarrow 2\,^1P$) and 4388-Å ($5\,^1D \rightarrow 2\,^1P$) He I lines. For the upper levels in these two cases, the only states which need be included in calculations for electric fields $E_{\rm rms} < 20$ kV/cm and frequencies ω, $\omega_L < 75$ GHz are the $4P$, D, and F, and the $5P$, D, F, and G, respectively. The lower states ($n = 2$) are negligibly affected by the electric field because the $2P$, $m = 0, \pm 1$ states are not coupled by the $\beta^{\pm}$ matrix elements and the $2P$ levels are widely separated from any other levels. However, the $2P$ levels are split by the magnetic field.

For our calculations, we have used Martin's values[19,20] for the eigenvalues of H_0, and hydrogen-like eigenfunctions for the $\{U_j\}$.

In the calculations which are presented below, we have *not* included a magnetic field. This is because a thorough treatment of the effects of a magnetic field was given in Sec. III and the new phenomena which arise when the perturbation treatment is not valid are similar to those which are shown below for the case of electric field alone. That is, higher-order satellites and Stark shifts become important.

Figures 2 and 3 show calculated Stark profiles of

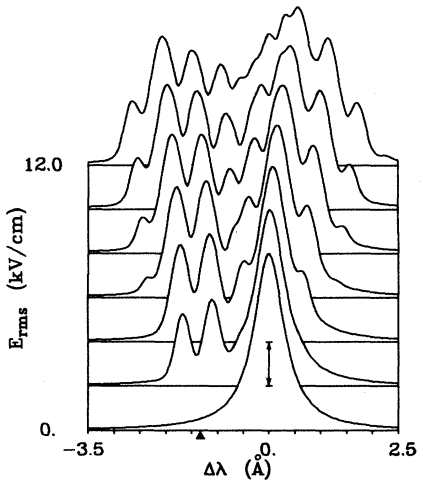

FIG. 2. Calculated Stark profiles in the vicinity of the 4922-Å spectral line of He I for the case of no magnetic field and a linearly polarized electric field of frequency 1.17 cm^{-1} and for various electric field strengths, all for direction of observation perpendicular to $\vec{E}$. Each profile is the result of folding the theoretical line spectrum with an instrument function of FWHM of 0.2 Å and is shown plotted logarithmically; a single decade is shown in the figure by a double-ended arrow. $\Delta\lambda = 0$ is the unperturbed position of the allowed line $4\,^1D \rightarrow 2\,^1P$; ▲ denotes the unperturbed position of the forbidden transition $4\,^1F \rightarrow 2\,^1P$.

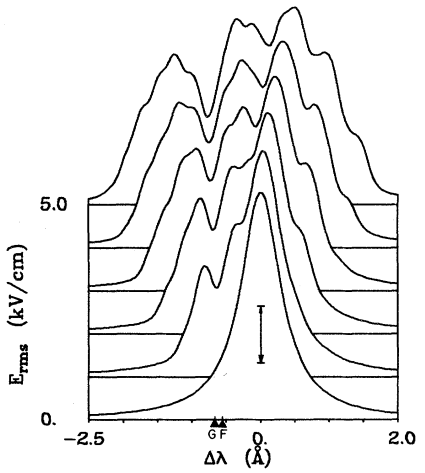

FIG. 3. Calculated Stark profiles in the vicinity of the 4388-Å spectral line of He I for the case of no magnetic field and a linearly polarized electric field of frequency 1.17 cm^{-1} and for various electric field strengths, all for direction of observation perpendicular to $\vec{E}$. Each profile is the result of folding the theoretical line spectrum with an instrument function of FWHM of 0.2 Å and is shown plotted logarithmically; a single decade is shown in the figure by a double-ended arrow. $\Delta\lambda = 0$ is the unperturbed position of the allowed line $5\,^1D \rightarrow 2\,^1P$; $\blacktriangle_F$ and $\blacktriangle_G$ denote the unperturbed positions of the forbidden transitions, $5\,^1F \rightarrow 2\,^1P$ and $5\,^1G \rightarrow 2\,^1P$, respectively.

He 4922 Å and He 4388 Å for an electric field frequency of 35.1 GHz (1.17 cm^{-1}) for various field strengths. This frequency was used because it is the one used in the experiment described in Sec. V. In the calculations we have set $S = 10$ for $E_{rms} \leq 6$ kV/cm and $S = 15$ for stronger fields. The resulting matrix $\underline{X}$ has then been numerically diagonalized using a CDC 6600 computer. Since for strong electric fields there are a great many satellites which contribute significantly to the spectrum, the main features of the spectrum are more easily seen if the multitude of theoretical lines predicted by our calculations are "smoothed" by folding with an "instrument" function. To obtain the profiles shown in the figures we have used the function

$$I = 10^{-4x^2/(x^2+a^2)},$$

where x is the distance in angstroms from a line center and a has been set to give a full width at half-maximum of 0.2 Å. This instrument function produces a line shape which is often observed experimentally for nonhydrogenic lines: Gaussian at the center and Lorentzian in the wings, with a weak continuum background. The half-width and background chosen are approximately those of the experiment described in Sec. V. In each figure the profiles are plotted lined up behind each other and the intensity of each profile is plotted logarithmically. The first profile in each figure is the instrument function, the profile for no electric field.

For low field strengths the profiles calculated by using the multilevel theory of Sec. II agree with the perturbation theory: The pattern consists of a strong allowed line and "far" and "near" satellites separated by twice the field frequency. For higher electric field strengths other satellites appear and grow until they dominate the spectral pattern. The additional satellites are due to multiple photon transitions from the upper set of states to the $2P$ level. In Fig. 2 the allowed line ($4\,^1D \rightarrow 2\,^1P$) has satellites associated with it which are due to an even number of photons being absorbed or emitted from the external field, while the forbidden transition ($4\,^1F \rightarrow 2\,^1P$) has associated with it satellites due to an odd number of photons being emitted or absorbed; these additional satellites are separated from the positions of the corresponding transitions by even and odd multiples of the field frequency, respectively. Figure 2 also shows the effect of the Stark shift of the $4D$ and $4F$ levels: The satellites of the forbidden line and the satellites of the allowed line (as well as the allowed line itself) appear to "repel" each other as the field strength is increased. The allowed line and its satellites are shifted towards longer wavelengths and the satellites of the forbidden line are shifted towards shorter wavelengths.

The spectra shown in Fig. 3 for the 4388-Å line are more complex than those of Fig. 2 due to coupling of the $5\,^1D$ and $5\,^1F$ levels to the nearby $5\,^1G$ level. This coupling not only modifies the positions and intensities of satellites arising from the $5\,^1D$ and $5\,^1F$ levels but also produces an additional group of

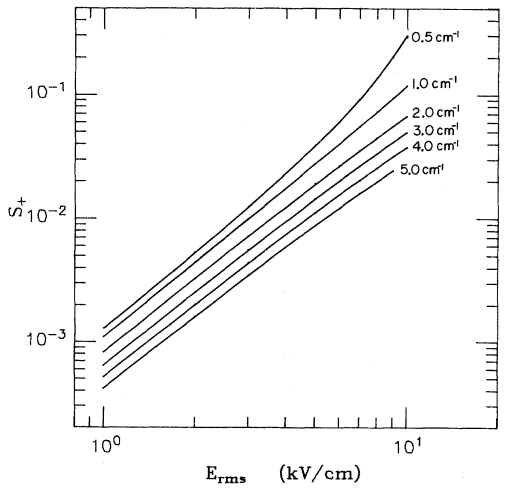

FIG. 4. Calculated intensity ratio S_+ of the far satellite of the forbidden transition $4\,^1F \rightarrow 2\,^1P$ to the allowed line $4\,^1D \rightarrow 2\,^1P$ in He I as a function of rms electric field strength for several electric field frequencies, for a linearly polarized electric field $\vec{E}$, and for direction of observation perpendicular to $\vec{E}$.

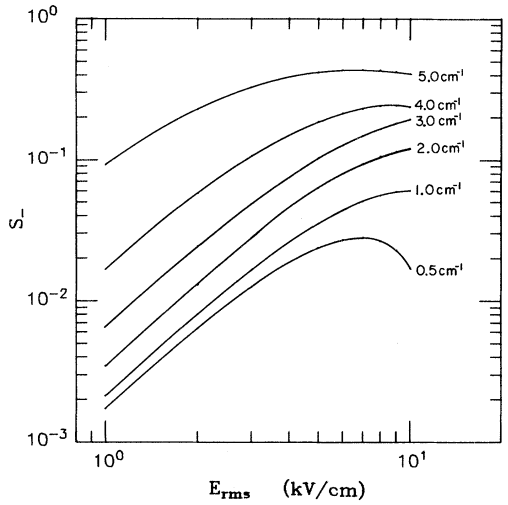

FIG. 5. Calculated intensity ratio S_- of the far satellite of the forbidden transition $4^1F \rightarrow 2^1P$ to the allowed line $4^1D \rightarrow 2^1P$ in He I as a function of rms electric field strength for several electric field frequencies, for a linearly polarized electric field $\vec{E}$, and for direction of observation perpendicular to $\vec{E}$.

satellites associated with the forbidden transition ($5^1G \rightarrow 2^1P$) and separated from it by even multiples of the field frequency. The Stark shift of the 5^1G level and its associated satellites is in the same sense as that of the 5^1F level, i.e., toward shorter wavelengths and "away" from the red-shifted allowed line.

In the limit of very strong electric fields, where the Stark shift is much greater than the unperturbed energy level separation, we expect the Stark patterns to approximate the symmetric patterns predicted by Blochinzew[21] for degenerate levels. Such a tendency can be seen in Fig. 2 where the spectrum becomes more symmetric as the 4^1D and 4^1F levels become increasingly "degenerate."

Figures 4 and 5 show the results of further calculations on the 4922-Å He I line, again with a linearly polarized electric field and no magnetic field. Because we have chosen the electric field polarized parallel to the z axis, each satellite and the allowed line have three uncoupled components whose amplitudes and Stark shifts depend upon the absolute value of m, the azimuthal quantum number. In calculating the data for these graphs we summed the amplitudes of the three components of the appropriate line.

In Figs. 4 and 5 the rms electric field is plotted against S_+ (S_-), the ratio of the far (near) satellite to the allowed line, for various frequencies (labeled in inverse centimeters). Perturbation theory predicts straight lines on a log-log plot (S_+ and S_- are each proportional to E^2_{rms}) which are tangent to the curves of Figs. 4 and 5 at low electric fields. For stronger fields there are increasing deviations from the results of perturbation theory. Figures 4 and 5, and also Fig. 2, show that the intensity of the far satellite is growing faster than the intensity of the near satellite, until at about 12 kV/cm the far satellite is actually stronger. As is noted in Ref. 11, and is clear from Figs. 4 and 5, the near satellite deviates much more than the far satellite from the predictions of perturbation theory, and the effects of the higher-order terms are to decrease the amplitude of the near satellite relative to the perturbation theory results.

From Figs. 4 and 5 it is in principle possible to determine the frequency and amplitude of an electric field from an experimentally measured spectrum. However, the appearance of additional satellites may confuse the spectral pattern even for relatively low field strengths.

For instance, consider Fig. 6, which shows a set of profiles of the 4922-Å line of He I for a frequency of 4.0 cm^{-1}. It is not clear from the figure which are the far and the near satellites even for weak electric fields. The line marked with an arrow is actually a satellite of the allowed line. Another situation where confusion could result is at very low frequencies, since the two satellites will then merge into a single line at the position of the forbidden line. Furthermore, in a plasma the forbidden line is always present due to the quasistatic Coulomb fields of the ions and it may be confused with the satellites if its intensity is compar-

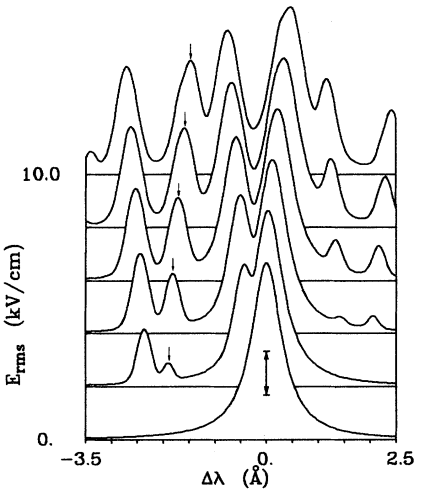

FIG. 6. Calculated (instrument-broadened) Stark profiles in the vicinity of the 4922-Å spectral line of He I for the case of no magnetic field and a linearly polarized electric field of frequency 4.0 cm^{-1} and for various electric field strengths, all for direction of observation perpendicular to $\vec{E}$. Each profile is plotted logarithmically; a single decade is shown by the double-ended arrow. $\Delta\lambda = 0$ is the unperturbed position of the allowed line $4^1D \rightarrow 2^1P$ and the single-ended arrow denotes one of its satellites.

able to satellite intensities. One might also see only a single satellite if the field frequency is close to the energy separation of the $4D$ and $4F$ levels; then the near satellite will be buried in the "wings" of the allowed line. For these reasons we emphasize that unless the features of the spectrum are clearly identifiable, extreme caution must be observed in using the perturbation calculations or Figs. 4 and 5.

The amplitude of the electric field can also be determined by measuring the Stark shift of the lines.[14] It is usually most convenient to measure the total Stark shift, which we define as the change in the separation of the forbidden and allowed lines (compared with their separation with no external fields). The Stark shift of the allowed line can also be used if one can determine its unshifted position. For low fields Eq. (35) can be used to find the Stark shifts; for high fields the theory of Sec. II must be used. From Eq. (35) we can see that for linear polarization the Stark shift is proportional to

$$1/(\omega_{ij}'^2 - \omega^2) ,$$

and therefore for $\omega < |\omega_{ij}'|$ it is a rather weak function of the frequency. Thus in this case a precise knowledge of the frequency is unnecessary; for other polarizations, however, the dependence of the Stark shift on the frequency is stronger.

V. EXPERIMENT

We have experimentally studied the effect of a linearly polarized high-frequency electric field on eigenstates of He I by observing optical transitions in the vicinity of two allowed lines, which we will refer to as

case I: 4922 Å ($4\,^1D$, etc. $\rightarrow 2\,^1P$),

case II: 4388 Å ($5\,^1D$, etc. $\rightarrow 2\,^1P$),

and by comparing the observed spectrum with the spectrum calculated by using the methods of Secs. II and IV. In both cases there is *no* magnetic field. Figures 2 and 3 of Sec. IV show the theoretical profiles predicted by the multilevel theory of Sec. II for cases I and II for the experimentally measured electric field frequency and for various field strengths.

A. Apparatus

Figure 7 shows the apparatus used in the experiment. We generate the high-frequency electric field in a cylindrical microwave cavity and apply it to a helium plasma produced by a dc discharge in a quartz capillary which threads the axis of the cavity. The cavity (0.609 cm in diameter and 0.865 cm in length) oscillates in the TM_{010} mode with the electric field parallel to the axis of symmetry and electric field strength maximum along the axis of the cavity. Mode identification was verified by calculating the resonant frequency of cavity plus quartz capillary, which agreed to within 1% of the measured frequency, 35.2 GHz, and also by measuring the relative electric field intensity as a function of position along the axis of the cavity. This latter measurement was done by measuring the change in resonant frequency of the cavity–quartz-capillary system as a small quartz plug was pushed into the cavity down the inside of the quartz capillary. The calculated electric field intensity variation over the inside cross section of the capillary (o.d., 0.85 mm; i.d., 0.40 mm) is $< 5\%$ of the value on the axis. In operation with a plasma, helium flow is maintained continuously through the capillary: typically, the pressure at the high-pressure end of the capillary is 3 Torr, and pressure at the low-pressure end is 1 Torr. Other typical discharge parameters are current 3.5 mA; current density, 4 A/cm^2; average dc electric field strength, 300 V/cm; and electron density, 1×10^{11} cm^{-3}. The electron density is determined by measuring the change of resonant frequency of the microwave cavity due to the presence of the plasma. The field frequency is much greater than either the plasma frequency or the electron collision frequency, so that the microwave field has no noticeable effect on the plasma. Further details of the experimental arrangement are given in Ref. 3. Two changes should be noted, however. The cavity is now excited by a 10-W cw klystron. With the higher power and electric field the satellites are no longer buried in the wings of the allowed line; this permits the experiment to be run cw and obviates the need for phase-sensitive detection. The light intensity at a given wavelength is now measured by use of standard photon-counting techniques. Peak intensities in Figs. 8 and 9 represent $> 10^4$ counts/sec. For a single experimental point, counts were taken for 10 sec.

B. Comparison of Theory and Experiment

For a direct comparison of the theoretical calculations with our measured line profiles, we have folded the theoretical results, which consist of a discrete line spectrum, with a realistic "instrument function" obtained from measurements taken on the same apparatus but with the microwave power turned off. Most of the observed broadening was instrumental. Figures 8 and 9 show comparisons of experimental results with various theories, all calculated for observation at right angles to the direction of the electric field and for a peak field strength of 5.0 kV/cm (3.54 kV/cm rms). In all cases $\Delta\lambda = 0$ is the position of the allowed line in the absence of the perturbing electric field. All "bumps" on the theoretical profiles are produced by one or more satellites and not by irregularities

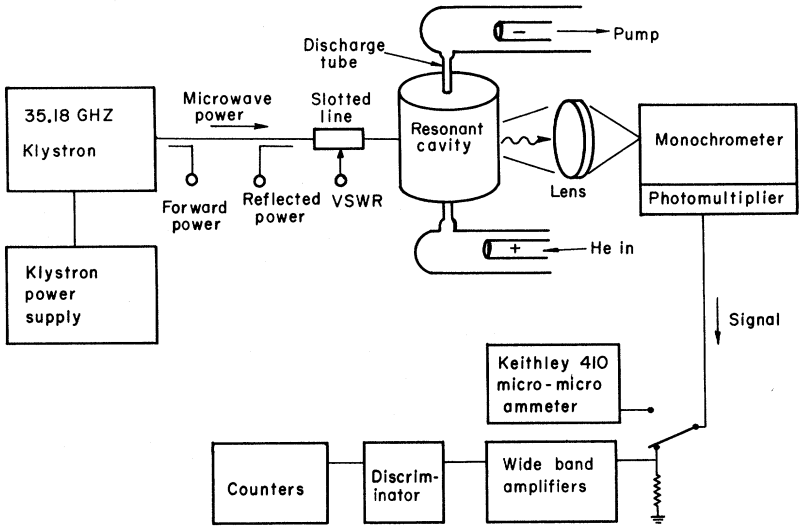

FIG. 7. Schematic diagram of the experiment.

in the instrument function. All satellites stronger than 10^{-5} of the total intensity of the pattern were retained in the calculations (the number of satellites so kept is noted in the discussion of each figure).

Figure 8 shows a comparison between experimental and theoretical results for case I. The multilevel theory outlined above, the Autler-Townes theory, and the perturbation theory of Baranger and Mozer all give nearly the same results for the predicted spectrum; the major discrepancy between them comes from the neglect of the Stark shift in the perturbation calculation. The slight difference between the Autler-Townes and the multilevel theories is due to the retention of the $4P$ energy level in the latter. In both cases we have included 18 satellites. Agreement of the multilevel theory with experiment is excellent, and even the other two theories agree quite well with experiment for this field strength. The close agreement of the perturbation calculations and the multilevel calculations, which we expect to be much more accurate, indicate that the perturbation calculations can still be trusted for this line at this frequency and field strength. The value so obtained was 5 kV/cm peak field with an estimated error of less than 500 V/cm.

Case II, shown in Fig. 9, is a much more severe test of the various theories owing to the following: (a) The matrix elements $\beta^{\pm}$ increase with n, hence the effect of a given electric field is greater on the 4388-Å line than on the 4922-Å line. (b) The energy levels of $n = 5$ are closer together, so that more satellites (i.e., higher-order transitions) become important. (c) For $n = 5$ there is a G energy level very near the F energy level, and the two interact strongly.

In Fig. 9 we compare the measured line profile for the 4388-Å line with theoretical ones calculated from our multilevel theory and from the Autler-Townes theory, using the field strength derived from the measurements on the 4922-Å line. Agreement between the multilevel calculations and the measured data is very good, whereas experiment and the Autler-Townes calculations sharply disagree, not only in satellite positions and intensities but also in the Stark shift of the allowed line. This disagreement graphically illustrates the need to include additional upper levels, since this is the only significant difference in the two theories.

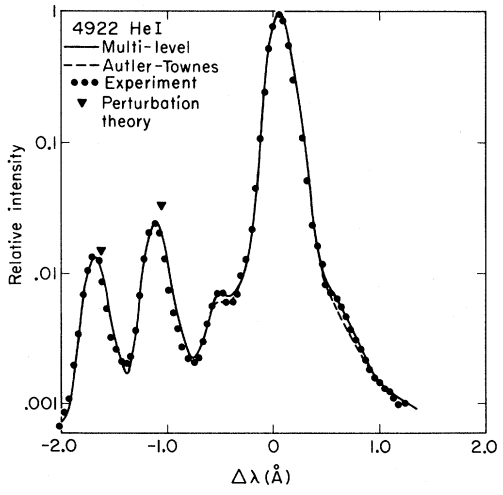

FIG. 8. Comparison of experiment and various theories for case I ($4\,^1D$, etc. $\rightarrow 2\,^1P$), 4922-Å He I for the case of no magnetic field and a linearly polarized electric field of frequency 1.17 cm^{-1} and rms electric field strength of 3.54 kV/cm, and for direction of observation perpendicular to the electric field.

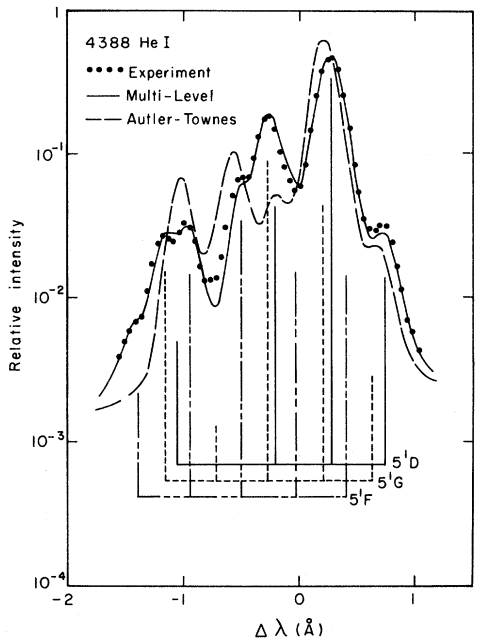

FIG. 9. Comparison of experiment and various theories for case II ($5\,^1D$, etc. $\rightarrow 2\,^1P$), 4388-Å He I for the case of no magnetic field and a linearly polarized electric field of frequency 1.17 cm^{-1} and rms electric field strength of 3.54 kV/cm, and for direction of observation perpendicular to the electric field. The sets of vertical lines labeled $5\,^1D$, $5\,^1F$, and $5\,^1G$ indicate the positions and relative intensities of spectral components originating from those levels.

Perturbation calculations, not shown, disagree even more strongly with measurements. In the Autler-Townes calculations we include 42 satellites; 58 were used in the multilevel calculations.

In Fig. 9 we have also indicated the major satellites originating from the three upper levels, $5\,^1D$, $5\,^1F$, and $5\,^1G$. Each vertical line in the figure denotes the average position and relative intensity of the narrowly separated satellites which result from transitions from upper levels with differing magnetic quantum numbers.

ACKNOWLEDGMENTS

The authors wish to thank Professor W. B. Kunkel and the other members of the Berkeley plasma physics group for many helpful discussions during the course of this work. We are especially grateful to Peter S. Rostler whose critical reading of the rough drafts of this paper has been invaluable and to E. B. Hewitt for his assistance on the experiment.

APPENDIX

A. Calculation of Transition Rate for Atom in Static Magnetic Field and Oscillating Electric Field

In order to calculate the theoretical radiation pattern emitted by an atom in an oscillating electric field we solve the equation

$$i\frac{\partial\Phi}{\partial t} = [H(t)+H']\Phi\,, \tag{A1}$$

where $H(t)$ is as defined in Eq. (1) and H' is the particle-radiation field interaction operator

$$H' = \frac{e}{\hbar m_e c}\,\vec{A}\cdot\left(\vec{p}+\frac{e}{c}\,\vec{A}^{ex}\right);$$

$\vec{p}$ is the momentum of the optical electron, $\vec{A}$ is the vetor potential of the radiation field, and $\vec{A}^{ex}$ is the vector potential of the external magnetic field. At any time t, the solutions of the equation $i(\partial\varphi/\partial t) = H(t)\varphi$ form a complete orthnormal set. Hence we may expand $\Phi(t)$ as $\Phi(t) = \sum_d \Gamma_d(t)\varphi_d(t)$, where the sum is over the complete set of the φ's. The φ's explicitly contain both atomic and radiation field quantum numbers and hence differ from the solutions of Eq. (1) (ψ's). Substitution for $\Phi(t)$ in Eq. (A1) yields

$$i\sum_d \frac{d\Gamma_d}{dt}\,\varphi_d = \sum_d \Gamma_d H'\varphi_d\,. \tag{A2}$$

Multiplication of Eq. (A2) on the left-hand side by φ_k^* and integration over all space yields an equation governing the time development of the coefficient Γ_k:

$$i\frac{d\Gamma_k}{dt} = \sum_d \langle k|H'|d\rangle\,\Gamma_d\,; \tag{A3}$$

the matrix element $\langle|H'|\rangle$ involves integration over both atomic and radiation field variables.

We assume that at $t=\tau$ the system (atom + radiation field) is in a state $\Phi = \varphi_i\,[\,\Gamma_d(\tau) = \delta_{di}\,]$; then $|\,\Gamma_k(t)\,|^2$ is the probability that the system, initially in state i at $t=\tau$, will by time t have undergone a transition to state k by emitting or absorbing photons from the radiation field. If we consider a time interval, $t-\tau$, small compared with the lifetime of state i, then we can solve Eq. (A3) by iteration:

$$\Gamma_k = \Gamma_k^{(0)} + \Gamma_k^{(1)} + \cdots, \quad \Gamma_k^{(0)} = \delta_{ki}\,,$$
$$\Gamma_k^{(1)} = -i\int_\tau^t dt\,\langle k|H'|i\rangle, \text{ etc.} \tag{A4}$$

We now specialize to the problem of spontaneous emission of a single photon γ in the atomic transition $\psi_i \rightarrow \psi_k$, where ψ_i and ψ_k are given by Eq. (14) and Eq. (22). Then we have

$$\varphi_k = e^{-i(\omega_\gamma+\omega_k')t}\,U_k(\vec{r})\,\Lambda_\gamma\,,$$

$$\varphi_i = e^{-i\lambda_i t}\sum_{j=1}^{N}\sum_{s=-\infty}^{\infty} C_{js}^{i}\,e^{-is\omega t}\,U_j(\vec{r})\,\Lambda_0\,,$$

where Λ is the radiation field state function; Λ_γ

denotes the presence of photon γ; Λ_0 denotes that no such photon is present. By substituting φ_k and φ_i into Eq. (A4) and performing the time integration we have

$$|\Gamma_k^{(1)}|^2 = \sum_{j=1}^{N}\sum_{j'=1}^{N}\langle j'|H'|k\rangle\langle k|H'|j\rangle \sum_{s=-\infty}^{\infty}\sum_{s'=-\infty}^{\infty} C_{js}^{i} C_{j's'}^{i*}\, e^{-(1/2)i[(s-s')\omega(t+\tau)]} \times \frac{4\sin\frac{1}{2}[(\omega_\gamma+\omega_k'-\lambda_i-s\omega)(t-\tau)]}{(\omega_\gamma+\omega_k'-\lambda_i-s\omega)} \frac{\sin\frac{1}{2}[(\omega_\gamma+\omega_k'-\lambda_i-s'\omega)(t-\tau)]}{(\omega_\gamma+\omega_k'-\lambda_i-s'\omega)} ,$$

where the matrix element $\langle|H'|\rangle$ now denotes integration only over atomic variables.

As a function of ω_γ, $|\Gamma_k^{(1)}|^2$ consists of a series of "peaks" with centers $\omega_\gamma = \lambda_i + s\omega - \omega_k'$ and widths $\approx 1/(t-\tau)$. For $\omega(t-\tau) \gg 1$ the peaks are narrow relative to the interpeak spacing ω and we can approximate $|\Gamma_k^{(1)}|^2$ by

$$|\Gamma_k^{(1)}|^2 \simeq \int d\omega_\gamma \sum_{s=-\infty}^{\infty} \delta(\omega_\gamma+\omega_k'-\lambda_i-s\omega) I_k^{is} ,$$

where I_k^{is} is the number of photons emitted in transitions from state i to state k into solid angle $d\Omega$ with $\omega_\gamma \simeq \lambda_i + s\omega - \omega_k'$ during the time interval (τ, t):

$$I_k^{is} \equiv \int_{\omega_-}^{\omega_+} d\omega_\gamma |\Gamma_k^{(1)}|^2 \rho(\omega_\gamma) d\Omega = 2\pi \sum_{j=1}^{N}\sum_{j'=1}^{N}\langle j'|H'|k\rangle\langle k|H'|j\rangle \sum_{s'=-\infty}^{\infty} C_{js}^{i} C_{j's'}^{i*} \times \frac{e^{-i\omega(s-s')\tau} - e^{-i\omega(s-s')t}}{i(s-s')\omega} \rho(\omega_\gamma) d\Omega ;$$

$\rho(\omega_\gamma)$ is the density of photon states per radian solid angle and $\omega_\pm = \lambda_i + s\omega - \omega_k' \pm \Delta$, where Δ is chosen to satisfy $1/(t-\tau) \ll \Delta \ll \omega$. In performing the integrations above we have used the sharply peaked nature of the integrands by evaluating $\rho(\omega_\gamma)$ and the matrix elements at the peak center and then letting $\Delta \to \infty$. Of more physical interest than $|\Gamma_k^{(1)}|^2$ is its time derivative, the differential transition rates:

$$\frac{d}{dt}|\Gamma_k^{(1)}|^2 = 2\pi \int d\omega_\gamma \sum_{j=1}^{N}\sum_{j'=1}^{N}\langle j'|H'|k\rangle\langle k|H'|j\rangle \times \sum_{s=-\infty}^{\infty}\sum_{s'=-\infty}^{\infty} C_{js}^{i} C_{j's'}^{i*}\, \rho(\omega_\gamma) d\Omega \times [e^{-i(s-s')\omega t}\, \delta(\omega_\gamma+\omega_k'-\lambda_i-s\omega)]. \tag{A5}$$

The differential transition rate given by Eq. (A5) is a rapidly varying function of time for frequencies for which the approximations above hold [$\omega \gg (t-\tau)^{-1} \gg$ (lifetime of state i)$^{-1}$], and hence of more experimental interest is the time-averaged differential transition rate dA_i^k. Evaluation of the matrix elements in Eq. (A5) (using the dipole approximation) and $\rho(\omega_\gamma)$ yields

$$\langle k|H'|j\rangle = i(2\pi e^2/\hbar v\omega_\gamma)^{1/2}\, \omega_{jk}' \xi_j^k ,$$

$$\rho(\omega_\gamma) = v\omega_\gamma^2/8\pi^3 c^3 ,$$

where v is the system volume, the magnetic field has been assumed to lie in the $+z$ direction, and where we have defined the following quantities:

$$\omega_{jk}' \equiv \omega_j' - \omega_k', \quad \omega_j' \equiv \int d^3r\, U_j^* (H_0 + H_1) U_j, \text{ etc.}$$

$$\xi_j^k \equiv \int d^3r\, U_k^*\, \hat{e}_\gamma^* \cdot \vec{r}\, U_j .$$

Then we have

$$dA_i^k = \int d\omega_\gamma \frac{e^2 d\Omega}{2\pi\hbar c^3} \sum_{s=-\infty}^{\infty} \omega_\gamma \delta(\omega_k' + \omega_\gamma - \lambda_i - s\omega) \times \sum_{j=1}^{N}\sum_{j'=1}^{N} \omega_{jk}' \omega_{j'k}' \xi_j^k \xi_{j'}^{k*} C_{js}^{i} C_{j's}^{i*} . \tag{A6}$$

The integrand of expression (A6) gives the photon emission spectrum $\mathcal{S}(\omega_\gamma)$:

$$\mathcal{S}(\omega_\gamma) = \frac{e^2}{2\pi\hbar c^3} \sum_{s} \omega_\gamma \delta(\omega_k' + \omega_\gamma - \lambda_i - s\omega) \times \sum_{j=1}^{N}\sum_{j'=1}^{N} \omega_{jk}' \omega_{j'k}' \xi_j^k \xi_{j'}^{k*} C_{js}^{i} C_{j's}^{i*} . \tag{A7}$$

B. Weak-Field Limit

If the electric field is weak, then we can get an explicit expression for the solution of Eq. (53). We set $S = 1$ (higher values correspond to multiple quantum transitions which we expect to be rare for weak electric fields) and diagonalize the matrix $\underline{X}$. The resulting expression for λ and the C's are power series in the small parameters $\beta_{ij}^{\pm}$:

$$\lambda_i = \omega_i' + \omega_i^S + O(|\beta|^3) ,$$

$$C_{js}^{i} = \delta_{s0}\delta_{ij} + \frac{\delta_{s1}\beta_{ji}^{-}}{(\omega_{ij}' + \omega)} + \frac{\delta_{s,-1}\beta_{ji}^{+}}{(\omega_{ij}' - \omega)} + O(|\beta|^2),$$

$$\omega_i^S \equiv \sum_j \frac{|\beta_{ji}^{-}|^2}{(\omega_{ij}' + \omega)} + \frac{|\beta_{ji}^{+}|^2}{(\omega_{ij}' - \omega)} ; \tag{A8}$$

ω_i^S is the Stark shift of level i due to the electric field and is quadratic in the electric field amplitude.

In deriving the above expressions we had to assume $|\beta^{\pm}_{ij}| \ll |\omega'_{ij}|$, and also that $|\omega'_{ij} \pm \omega| \gg O(|\beta|)$; these assumptions will be discussed in Sec. C of the Appendix.

The resulting expressions for the $\mathcal{S}(\omega_\gamma)$ will contain cross terms of the form $\xi^k_j \xi^{k*}_{j'} \beta^{\pm}_{ji} \beta^{\pm *}_{j'i}$. In many cases of physical interest (discussed in Sec. C of the Appendix) $\xi^k_j \xi^{k*}_{j'} \beta^{\pm}_{ji} \beta^{\pm *}_{j'i} \propto \delta_{jj'}$. In this case Eq. (A7) reduces to

$$\mathcal{S}^k_i(\omega_\gamma) = \frac{e^2}{2\pi\hbar c^3}\left[\omega_\gamma^3\,\delta(\omega_\gamma - \omega'_{ik} - \omega^S_i)\,|\xi^k_i|^2 + \omega_\gamma \delta(\omega_\gamma - \omega'_{ik} - \omega^S_i - \omega)\sum_j \frac{|\xi^k_j|^2 |\beta^-_{ji}|^2 \omega'^2_{ji}}{(\omega'_{ij} + \omega)^2} + \omega_\gamma \delta(\omega_\gamma - \omega'_{ik} - \omega^S_i + \omega)\sum_j \frac{|\xi^k_j|^2 |\beta^+_{ji}|^2 \omega'^2_{ik}}{(\omega'_{ij} - \omega)^2}\right] + O(|\beta|^4). \quad \text{(A9)}$$

The spectrum given by expression (A9) consists of three spectral lines: a line resulting from a dipole transition from i to k with resulting photon energy $\omega_\gamma = \omega'_{ik} + \omega^S_i$, and two weaker "satellites" with energies $\omega_\gamma = \omega'_{ik} + \omega^S_i \pm \omega$ which result from two-quantum transitions (one quantum absorbed from or emitted to the electric field). If a dipole transition from i to k is forbidden ($\xi^k_i = 0$), but the dipole matrix elements $\beta^{\pm}_{ji}$ and ξ^k_j are nonzero, then the spectrum is composed of just the two satellites and we have Eq. (34). If $\xi^k_j \neq 0$ then, to lowest order, $\mathcal{S}(\omega_\gamma)$ is just the usual spectrum for an "allowed" dipole transition from i to k.

C. Validity of Perturbation Theory

We now discuss the assumption made in deriving Eq. (A9).

(i) The form of Eq. (A9) depends on the assumption that the cross terms of the form

$$\omega'_{jk}\,\omega'_{j'k}\,\frac{\beta^{\pm}_{ij}\beta^{\pm *}_{ij'}\xi^k_j \xi^{k*}_{j'}}{(\omega'_{ij} \pm \omega)(\omega'_{ij'} \pm \omega)}, \quad j \neq j'$$

can be ignored in the final expression for the spectrum $\mathcal{S}$. Before discussing situations in which this assumption holds, we note that due to the form of the denominators in Eq. (A9), the leading contribution to the satellite intensities and positions will come from terms in the sums involving intermediate states whose energies lie close to the energy of state i. More distant states will have less effect and states for which the energy separation ω'_{ij} is much greater than the energy separation of the nearest states can be ignored in computing the satellite intensities and positions. Similarly, cross terms for which j and j' do not both represent states near to the state i can be ignored, since they will not significantly modify the result given in Eq. (A9) for the frequency spectrum.

We can identify two cases in which the assumption that the cross terms are negligible is valid.

(a) First, if for a given initial state i and final state k there exists only a single intermediate state j which is "near" to the state i and for which the matrix elements ξ^k_j and $\beta^{\pm}_{ij}$ are *both* nonzero, then the assumption is valid. This situation occurs for the singlet helium lines 4388 Å ($5^1D \rightarrow 2^1P$) and 4922 Å ($4^1D \rightarrow 2^1P$) for a linearly polarized electric field with either no magnetic field or polarized along the magnetic field, or an electric field circularly polarized perpendicular to the magnetic field. In the above cases, for a proper choice of coordinate system, each initial state (n, $l=3$, $m=-3, \cdots, 3$) is coupled to only a single one of the nearby intermediate states ($n, l=2$, $m=-2, \ldots, 2$) by the matrix element $\beta^{\pm}_{ij}$.

(b) Second, cross terms can be ignored when the time-averaged electric field is axially symmetric with respect to the magnetic field. Then, in a coordinate system with z axis along the magnetic field, the cross terms vanish when an average is taken over the aximuthal angles of the electric field and of the emitted photon.

(ii) $|\beta^{\pm}_{ij}| \ll |\omega'_{ij}|$, i.e., the weak-electric-field approximation. If the electric field is not weak then the problem must be solved numerically by the methods of Sec. II. The validity of the perturbation theory as the electric field increases is further discussed in Sec. IV.

(iii) $|\omega'_{ij} \pm \omega| \gg |\beta^{\pm}_{ij}|$. If this condition is violated then the perturbation expansion (A8) is no longer valid, since one of the "small" terms ($\propto \beta^{\pm}$) becomes comparable to the leading term. Since resonant denominators of the form $\omega'_{ij} \pm \omega$ also appear in the perturbation expressions for higher-order terms ($|s| > 1$), we can no longer be sure that the higher-order terms which were ignored in calculating Eq. (A8) will be weaker than the terms kept.

As noted by Autler and Townes,[4] perturbation theory also breaks down if a higher-order resonance condition is satisfied. If we consider the case most often used in plasma diagnostics where a dipole transition from $i \rightarrow k$ is forbidden and a dipole transition from $j \rightarrow k$ is allowed, then in the weak-electric-field limit for which perturbation theory is valid the condition for an nth-order resonance can be written as

$$\frac{1}{|\omega'_{ij}|}\,|\omega'_{ij} + \omega^S_i - \omega^S_j \pm n\omega| \lesssim \left(\frac{|\beta^{\pm}_{ij}|}{|\omega'_{ij}|}\right)^n \equiv \epsilon^n, \quad n = 3, 5, \ldots .$$

As can be seen from the above resonance condition, an nth-order resonance occurs when the Stark-shifted position of the nth satellite of the forbidden transition $i \rightarrow k$ (the forbidden transition has only odd-numbered satellites) is separated

from the Stark-shifted position of the allowed line $j \rightarrow k$ by a distance of the order of $|\omega'_{ij}|\epsilon^n$. Then the intensity of this satellite (which would normally be much less than the intensity of the allowed line) can be comparable to the intensity of the allowed line. Numerical calculations show that when a resonance occurs two spectral lines separated by a distance of the order of $|\omega'_{ij}|\epsilon^n$ appear at approximately the position of the allowed line predicted by the perturbation theory. A similar situation occurs at the predicted positions of the far and near satellites, where a higher-order satellite of the allowed line (which has only even-numbered satellites) can be comparable in intensity to the generally much more intense first-order satellites. For weak electric fields the separation between the two lines in each pair is very small and will not be seen in a real experiment with finite resolving power and broadened spectral lines. For stronger electric fields, the separation will be observable only for the lowest-order resonances. If the separation cannot be resolved, then each pair will be observed as a single "satellite" with an intensity equal to the sum of the individual intensities and an average position given by an average of the position of each component weighted by its intensity; numerical calculations with the theory of Sec. II indicate that the sum intensity and average position are given correctly by Eq. (A9).

---

*Work performed under the auspices of the U. S. Atomic Energy Commission.

[1]M. Baranger and B. Mozer, Phys. Rev. 123, 25 (1961).

[2]J. Reinheimer, J. Quant. Spectry. Radiative Transfer 4, 671 (1964).

[3]W. S. Cooper III and H. Ringler, Phys. Rev. 179, 226 (1969).

[4]S. H. Autler and C. H. Townes, Phys. Rev. 100, 703 (1955).

[5]H.-J. Kunze and H. R. Griem, Phys. Rev. Letters 21, 1048 (1968).

[6]G. Baravian, R. Benattar, J. Bretagne, J. L. Godart, and G. Sultan, Phys. Letters 30A, 198 (1969).

[7]B. Ya'akobi and G. Bekefi, Phys. Letters 30A, 539 (1969).

[8]H.-J. Kunze, H. R. Griem, A. W. DeSilva, G. C. Goldenbaum, and I. J. Spalding, Phys. Fluids 12, 2669 (1969).

[9]W. S. Cooper III and R. A. Hess, Phys. Rev. Letters 25, 433 (1970).

[10]F. R. Scott, R. V. Neidigh, J. R. McNally, Jr., and W. S. Cooper III, J. Appl. Phys. 41, 5327 (1970).

[11]Y. Hamada, J. Phys. Soc. Japan 29, 463 (1970).

[12]G. V. Zelenin, A. A. Kutsyn, M. E. Maznichenko, O. S. Pavlichenko, and V. A. Suprunenko, Zh. Eksperim. i Teor. Fiz. 58, 1879 (1970) [Sov. Phys. JETP 31, 1009 (1970)].

[13]N. Ben-Yosef and A. G. Rubin, J. Quant. Spectry. Radiative Transfer 11, 1 (1971).

[14]W. S. Cooper and W. W. Hicks, Phys. Letters 33A, 188 (1970).

[15]H. Margenau and G. M. Murphy, *The Mathematics of Physics and Chemistry* (Van Nostrand, New York, 1949), pp. 80 and 81.

[16]H. A. Bethe and E. E. Salpeter, *Quantum Mechanics of One and Two Electron Atoms* (Springer, Berlin, 1957), pp. 253 and 254.

[17]J. Brochard and P. Jacquinot, Ann. Phys. (Paris) 20, 509 (1945).

[18]C. Deutsch, H. W. Drawin, L. Herman, and Nquyen-Hoe, J. Quant. Spectry. Radiative Transfer 8, 1027 (1968).

[19]W. C. Martin, J. Res. Natl. Bur. Std. (U.S.) A64, 19 (1960).

[20]W. C. Martin, J. Res. Natl. Bur. Std. (U.S.) A74, 699 (1970).

[21]D. I. Blochinzew, Physik. Z. Sowjetunion 4, 501 (1933).